PAPER • OPEN ACCESS

Numerical studies of fluid flow and heat transfer in microchannel heat sink with trapezoidal cavities, ribs and secondary channel

To cite this article: S A Razali *et al* 2021 *J. Phys.: Conf. Ser.* **2053** 012022

View the article online for updates and enhancements.

Numerical studies of fluid flow and heat transfer in microchannel heat sink with trapezoidal cavities, ribs and secondary channel

S A Razali[1], N A C Sidik [2]* and S N A Yusof [2]

[1] Faculty of Mechanical Engineering, Universiti Teknologi Malaysia, 81310 Skudai, Johor, Malaysia
[2] Malaysia – Japan International Institute of Technology (MJIIT), Universiti Teknologi Malaysia, Jalan Sultan Yahya Petra, 54100 Kuala Lumpur, Malaysia

*Corresponding author's email : Azwadi@utm.my

Abstract. In order to improve reliability and prevent premature failure, heat produced by electronic devices must be transfer efficiently. The microchannel heat sink appears to be the most reliable cooling technology to improve heat transfer performance. A new Microchannel Heat Sink (MCHS) design has been proposed with trapezoidal cavities, ribs and secondary channels. Fluid flow and heat transfer characteristics for Reynold numbers from 100 to 500 are numerically studied and analysed. Four microchannel heat sinks with various related geometry have been considered in this study, for instance, microchannel with rectangular ribs (TRAC-RR) and microchannel with trapezoidal cavities (TRAC). The finite volume method (FVM) is used to solve the governing equations, and the computations are performed using the SIMPLE algorithm. The present design's overall performance is evaluated using the friction factor, the Nusselt number, and performance evaluation criteria (PEC). The results show that the TRAC-RR-SC MCHS is the best design for the proposed design compared to the other four geometries, with a maximum PEC of 1.78. Additionally, the secondary flow field analyses visually show the hydraulic and thermal performance enhancements due to interruption, flow mixing and redevelopment of the thermal boundary layer.

1. Introduction

With the emergence of technology in recent years, microelectronic devices and chips are shrinking in size to maximise performance, which results in extremely high heat generation. Microdevices thermal management has become a hot subject that has intrigued the interest of a rising number of academics. MCHS single-phase liquid cooling has been known as one of the most efficient methods for microdevices cooling, with advantages such as compactness and ease of integration with microchips or high-density data storage systems [1]. The simple plain channel is incapable of meeting these need as the heat load rises and the temperature of microdevices is very limited.

Bargles [2] has classified a large number of augmentation techniques. There are three types of augmentation techniques: active methods, passive methods, and a combination of the two. On the other hand, passive methods have a broader application than active methods because they do not require external power. These methods include the use of MCHSs with grooves/cavities to improve heat transfer. Chai et al. [3] experimentally and numerically compared the convective heat transfer of MCHSs with various cavities. Thermal resistance, heat transfer, and pressure drop were all measured in the new microchannels and compared with the rectangular microchannel. The thermal boundary layer and

secondary flow improved the heat transfer. The combined cavity and ribs structure in MCHSs demonstrated its advantages for further heat transfer enhancement. Numerous researchers discovered that MCHSs with ribs and cavities on the sidewalls performed better due to jetting effects and vortexes [4,5]. Li et al. [6] Compared the microchannels without ribs or cavities, and results showed that the suggested design enhanced flow mixing by encouraging chaotic advection and jetting. Moreover, the microchannel presented shows a more uniform velocity and temperature at the heat sink substrate reduced which give better heat transfer performance. Japar et al. [7] explored the flow and heat transfer structure in MCHS with fins, cavities, and secondary channels, providing a low pumping power consumption with a high heat transfer rate. Numerous studies have been conducted to optimise the geometrical structure of microchannel heatsinks [8-10]. However, only few investigations existed on the effect of a combination of multiple passive technique, specifically combination of trapezoid cavities, rectangular ribs, and secondary channels have been reported.

Therefore, this paper aims to emphasise studying the effectiveness of microchannel heat sink hybrid designs with a secondary channel for high heat transfer rates and utilises the secondary channel's characteristics, allowing for a greater flow area and reducing the pressure drop. The performance evaluation criteria in this investigation are established on a comparison of the suggested design's performance with straight rectangular microchannel performance.

2. Physical model
The geometric of the TRAC-RR-SC microchannel heat sink's computational domain has been displayed in figure 1 (a), which is a symmetrical part of the whole MCHS. Figure 1 (b) and table 1 show the detailed structures of TRAC-RR-SC MCH. Four different configurations of microchannels (RC-RR, TRAC, TRAC-RR, TRAC-RR-SC) are developed to study the effect of cavities, rib and secondary channels on the fluid flow and heat transfer performance.

(a) Isometric View   (b) Top View
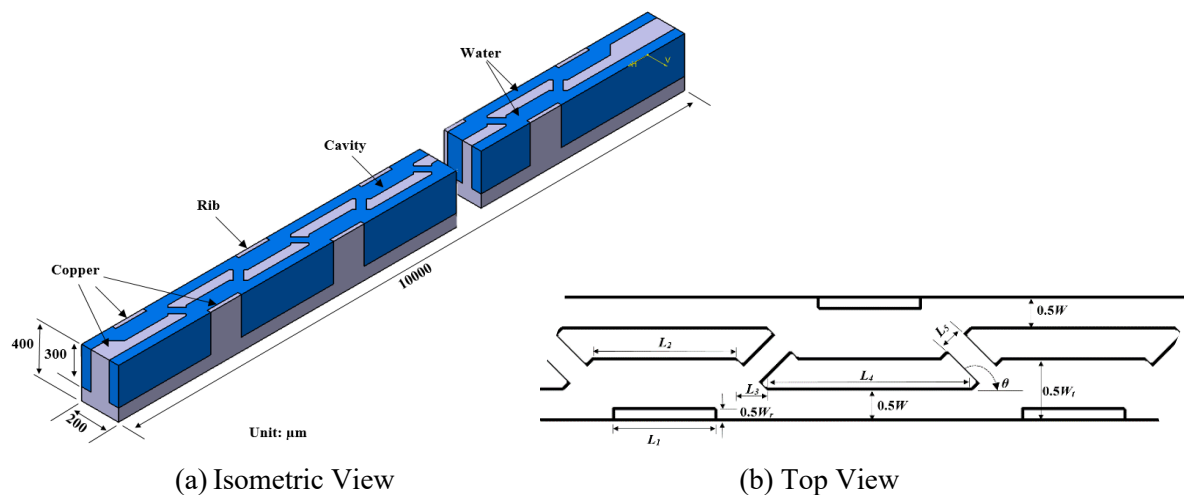
Figure 1. TRAC-RR-SC (a) Geometric of the computational domain (b) Structures of MCHS.

Table 1. List of a geometric dimensions of TRAC-RR-SC microchannels.

Parameters	Wt	W	Wr	L1	L2	L3	L4	L5	θ
Values, μm	300	150	56	250	350	75	500	60	45

3. Numerical Methods

3.1. Governing Equation

Continuity, momentum, and energy-governing equations in Cartesian coordinates in the nondimensional form are written as follows:

$$\frac{\partial u}{\partial x} + \frac{\partial v}{\partial y} + \frac{\partial w}{\partial z} = 0 \tag{1}$$

$$u\frac{\partial u}{\partial x} + v\frac{\partial u}{\partial y} + w\frac{\partial u}{\partial z} = -\frac{1}{\rho_f}\frac{\partial \rho}{\partial x} + \frac{\mu_f}{\rho_f}\left(\frac{\partial^2 u}{\partial x^2} + \frac{\partial^2 u}{\partial y^2} + \frac{\partial^2 u}{\partial z^2}\right) \tag{2}$$

$$u\frac{\partial v}{\partial x} + v\frac{\partial v}{\partial y} + w\frac{\partial v}{\partial z} = -\frac{1}{\rho_f}\frac{\partial \rho}{\partial y} + \frac{\mu_f}{\rho_f}\left(\frac{\partial^2 v}{\partial x^2} + \frac{\partial^2 v}{\partial y^2} + \frac{\partial^2 v}{\partial z^2}\right) \tag{3}$$

$$u\frac{\partial w}{\partial x} + v\frac{\partial w}{\partial y} + w\frac{\partial w}{\partial z} = -\frac{1}{\rho_f}\frac{\partial \rho}{\partial z} + \frac{\mu_f}{\rho_f}\left(\frac{\partial^2 w}{\partial x^2} + \frac{\partial^2 w}{\partial y^2} + \frac{\partial^2 w}{\partial z^2}\right) \tag{4}$$

$$u\frac{\partial T_f}{\partial x} + v\frac{\partial T_f}{\partial y} + w\frac{\partial T_f}{\partial z} = -\frac{k_f}{\rho_f c_{pf}}\left(\frac{\partial^2 T_f}{\partial x^2} + \frac{\partial^2 T_f}{\partial y^2} + \frac{\partial^2 T_f}{\partial z^2}\right) \tag{5}$$

$$0 = k_s\left(\frac{\partial^2 T_s}{\partial x^2} + \frac{\partial^2 T_s}{\partial y^2} + \frac{\partial^2 T_s}{\partial z^2}\right) \tag{6}$$

These assumptions are made to analyse the fluid flow and heat transfer in TRAC-RR-SC microchannel; 3D fluid flow, laminar, incompressible flow and steady-state, Newtonian, constant thermo-physical properties, velocity zero across solid boundaries, and negligible gravity and radiation heat transfer.

3.2 Boundary Condition and Grid Independence

A three-dimensional solid-fluid heat transfer numerical model has been created using Catia V5, and the numerical simulation has been performed using Fluent 17.0. In this investigation, copper MCHS is used with a constant wall heat flux of 1000 kW/m2 supplied to the substrate's bottom, and with an inlet temperature of 300 K, water is used as the working fluid. The average velocity at the entrance of the microchannel is fixed as 0.5–2.5 m/s for analysis. Figure 2 shows that Fluent 17 has generated a uniform grid throughout all zones.

The finite-volume method is used to discretized governing equations for all domains. The SIMPLEC algorithm is applied to resolve the coupling of velocity and pressure. Meanwhile, the second-order upwind scheme is set for the convective terms. Also, the second-order central difference scheme is selected for the diffusion term. The residual convergence criteria are set to be 10^{-6} for continuity and 10^{-9} for energy. To confirm mesh independence for the microchannel, the grid number of microchannel TRAC-RR-SC was varied between 0.6 million and 1.4 million when the Reynolds number was 500. The difference in relative error between the finest grids (J1) and the remainder of the grids (J2) is represented as (7)

$$e\% = \left|\frac{J_2 - J_1}{J_1}\right| \times 100 \tag{7}$$
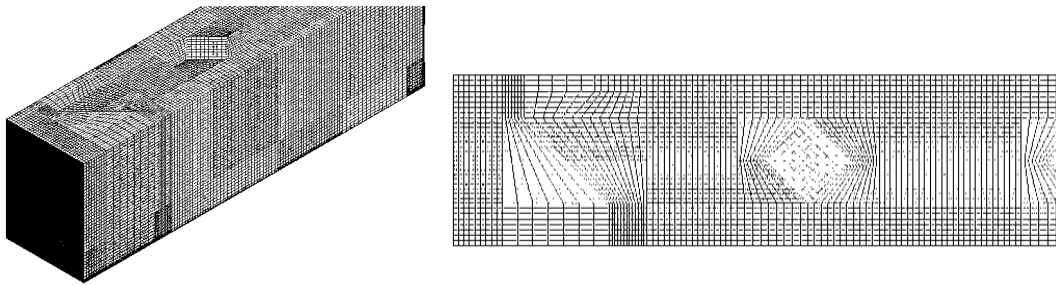
Figure 2. Three-dimensional grid diagram model.

According to table 2, the variations in Nusselt number and pressure drop are less than 0.91 percent. As a result, a grid number of 1.2 million is chosen to save computation time.

Table 2. Grid independence test.

Mesh	Nusselt.no	e%	Pressure drop	e%
1.4M	19.55	baseline	40267.46	baseline
1.2M	19.37	0.91	40216.34	0.12
1.0M	19.30	1.27	40152.01	0.28
0.8M	18.63	4.70	40115.25	0.37
0.6M	18.40	5.85	40095.73	0.42

3.3. Data Acquisition

The following equation calculates the Reynolds number (Re) and hydraulic diameter (Dh);

$$\text{Re} = \frac{\rho u_m D_h}{\mu} \tag{8}$$

$$D_h = \frac{2 H_c W_c}{H_c + W_c} \tag{9}$$

Where *Dh* is the hydraulic diameter in the microchannel. The friction factor is calculated from the pressure drop values using the equation below to assess hydraulic performance;

$$f_{app} = \frac{2 D_h \Delta P}{L_t \rho u_m^2} \tag{10}$$

Where *Lt* and *ΔP* are the total lengths of microchannel and pressure drop across the microchannel, the average heat transfer coefficient is calculated using the following formula:

$$h_{ave} = \frac{q_w A_{film}}{A_{con.} \left(T_{w,ave} - T_{f,ave} \right)} \tag{11}$$

$$Nu_{ave} = \frac{h_{ave} D_h}{k_f} \tag{12}$$

Where D_h, k_f, q_w, A_{film}, $A_{con.}$, $T_{w,ave}$ and $T_{f,ave}$ are the hydraulic diameter, the fluid's thermal conductivity, heat flux, the heated region, the convection heat transfer region, channel walls' average temperature and average fluid temperature.

A thermal-hydraulic performance evaluation criteria (PEC) index is performed to measure overall heat transfer performance while taking the pressure penalty into considerations which is defined as:

$$PEC = \frac{Nu / Nu_o}{\left(f / f_o\right)^{1/3}} \tag{13}$$

4. Results and Discussion

4.1 Validation

In order to analyse the accuracy of the numerical solution procedure, the present plain channel is firstly simulated and compared with the correlation given by Steinke and Kandlikar [8] and Darcy friction factor for the apparent friction factor. Figure 3(a) shows the plot of friction factor for Reynolds range of 100–500. The correlations are given by Steinke and Kandlikar [11] is expressed as (14-16), respectively.

$$f_{app} = f + \frac{\alpha(x)D_h}{L_t} \tag{14}$$

$$P_o = f\,\mathrm{Re} = 96[1 - 1.3553\left(AR\right) + 1.946\left(AR\right)^2 - 1.7012\left(AR\right)^3 + 0.9564\left(AR\right)^4 - 0.2537\left(AR\right)^5] \tag{15}$$

$$a(x) = 0.6796 + 1.2197\left(AR\right) + 3.3089\left(AR\right)^2 - 9.5921\left(AR\right)^3 + 8.9089\left(AR\right)^4 - 2.9959\left(AR\right)^5 \tag{16}$$

The Darcy friction factor is written as (17):

$$f_D = \frac{64}{\mathrm{Re}} \tag{17}$$

Meanwhile, the pressure drop is compared with correlations published by Steinke and Kandlikar [11] and displayed in figure 3(b). The pressure drop of the microchannel is defined as;

$$\Delta p = \frac{2\left(f\,\mathrm{Re}\right)\mu u_m L_t}{D_h} + \frac{a(x)\rho u_m^2}{2} \tag{18}$$

A good agreement is observed between the present model and theoretical data, as displayed in figure 3. It is clearly shown that the model data has very good matching with theoretical data. Thus, this numerical method can assess the performance of all designs in this current work.
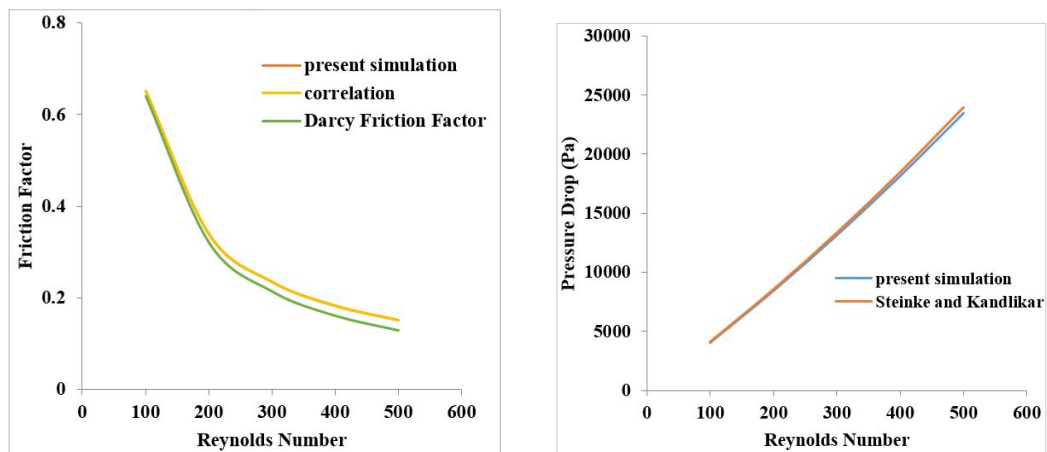
Figure 3. Comparison between the present model and theoretical data of (a) friction factor with correlation and (b) pressure drop with Steinke and Kandlikar [11].

4.2 Effects of trapezoidal cavities, ribs and secondary channel on heat transfer and fluid flow

Microchannel geometric configuration has a significant effect on the efficiency of fluid flow and heat transfer. The velocity and streamline are specified in the x–z plane (y = 0.25 mm) at Re = 500, respectively. As shown in figure 4, it can be obvious that the formation of cavities, ribs and secondary channel distinguishes the flow area from the rectangular channel (RC) where the streamlines are parallel. Fluid velocity constantly fluctuates and streams along the microchannel length because of the sudden expansion and blocking in the rib, cavities, and secondary channels.

The maximum velocity inside RC and trapezoidal cavities (TRAC) appear at the channel region's center. In contrast, the lowest flow velocity is discovered in the trapezoid cavities of TRAC channel, where the stagnation zone is located. The uniform velocity inside microchannels occurs at trapezoidal cavities-rectangular rib-secondary channel (TRAC-RR-SC). The velocity gradient is also elevated near the cavity, reflecting a stronger mix in the channel of near-wall hot fluid and center cold fluid. In the meantime, flow velocity has decreased in the downstream regions of the ribs.
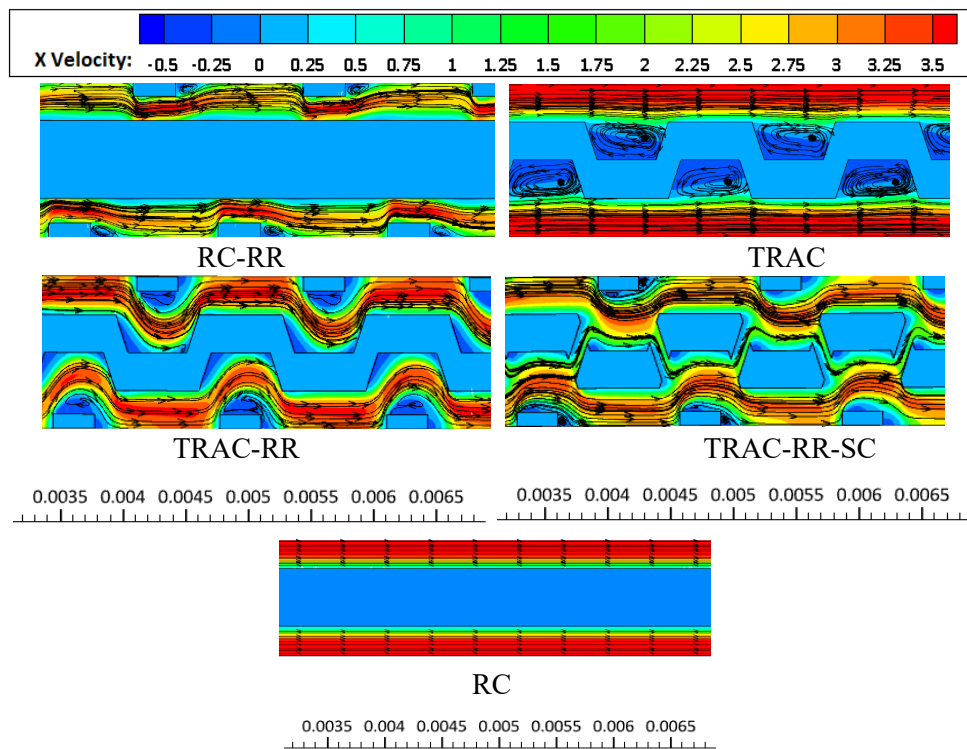
Figure 4. The velocity and streamline distributions for different structures on the x–z plane (y = 0.25 mm) at Re = 500.

4.3 Effect of trapezoidal cavities, ribs and secondary channel on microchannel performance

In the present investigation, the performance analysis parameters are focused on the differentiation of the suggested design performance with straight rectangular microchannel performance. The deviation of Nu/Nu_o and f/f_o with Reynolds number is shown in figures 5(a) and (b). The subscript (o) denotes rectangular microchannel RC. Basically, a higher Nusselt ratio will increase the performance, while a higher friction factor ratio will decrease the performance and vice versa.
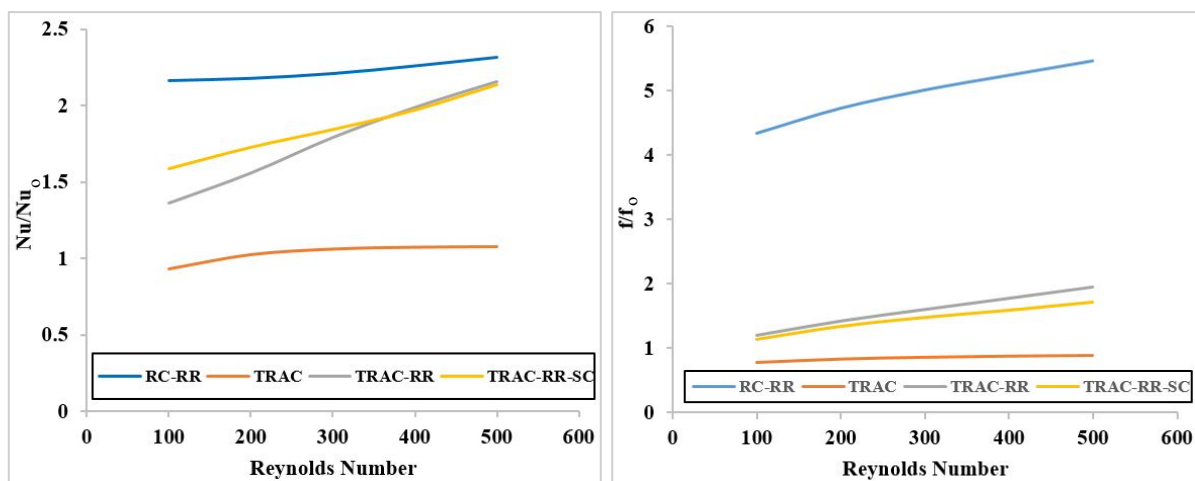

Figure 5. Variation of (a) Nu and (b) *f* with Reynolds Number for various geometries.

The best heat performance with a Nusselt ratio of 2.3 can be ascertained in rectangular-rectangular rib (RC-RR). Still, it also has the highest friction factor ratio due to the blocking rib configuration effect.

Meanwhile, TRAC shows the lowest thermal performance and the lowest friction factor ratio as a result of the stagnation zone found in cavities. Moreover, the secondary channels of TRAC-RR-SC greatly minimize the frictional loss incurred by ribs. It should be acknowledged that the friction loss average is 70% lower than RC-RR.

The overall performance of microchannels of different geometric configurations is now being compared using performance evaluation criteria (PEC). As mentioned in equation (13), this quantity indicates a thermal increase in hydrodynamic performance. The result shows PEC value is higher than one, which indicates that passive microstructures such as cavities, ribs, and secondary channels improve the heat sink's overall efficiency compared to simple microchannels. In figure 6, PEC variance is given within the Reynolds numbers $100 < Re < 500$ range for all configurations. Moreover, for trapezoidal channel-rectangular rib (TRAC-RR) and TRAC-RR-SC configurations, this performance criterion gradually increases as the Reynolds number increases.
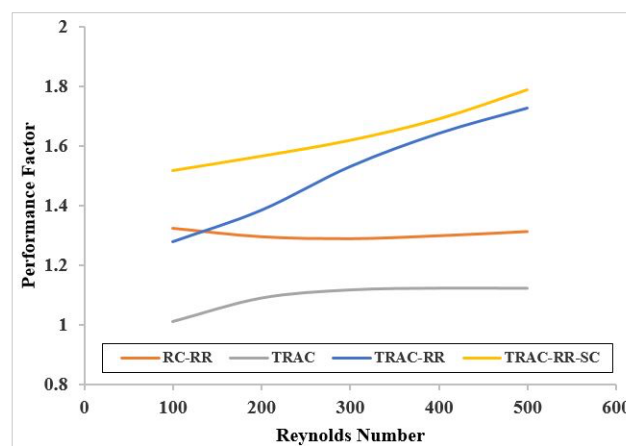
Figure 6. Variation of PEC with Reynolds Number for various geometries.

5. Conclusion

The effects of combining passive heat transfer methods, particularly cavities, ribs, and secondary channels on microchannel overall performance, were studied in this paper. Additionally, the fluid flow and heat transfer characteristics of the microchannel heat sink were numerically investigated. The main findings can be summarized that by combining passive heat transfer methods such as cavities, ribs, and secondary channels, hybrid techniques can significantly improve inclusive performance in microchannel heat sinks compared using individual techniques. The results show that the TRAC-RR-SC MCHS is the best design for the proposed design compared to the other four geometries, with a maximum PEC of 1.78.

6. References

[1]   Li S, Zhang H, Cheng J, Li X, Cai W, Li Z, and Li F 2019 A state-of-the-art overview on the developing trend of heat transfer enhancement by single-phase flow at micro scale *Int J Heat Mass Transf* **143** 118476

[2]   Bargles AE 1985 *Techniques to augment heat transfer. Handbook of Heat Transfer Applications* Ed W.M. Rohsenow, J.P. Hartnett, E.N. Ganic (New York: McGraw-Hill) Chapter 3 p 3-80

[3]   Chai L, Xia G, Wang L, Zhou M, and Cui Z 2013 Heat transfer enhancement in microchannel heat sinks with periodic expansion-constriction cross-sections *Int J Heat Mass Transf* **62(1)** 741–51

[4]   Bayrak E, Olcay AB, and Serincan MF 2019 Numerical investigation of the effects of geometric structure of microchannel heat sink on flow characteristics and heat transfer performance. Int J Therm Sci **135** 589–600

[5]   Zhai YL, Xia GD, Liu XF, and Li YF 2014 Heat transfer in the microchannels with fan-shaped reentrant cavities and different ribs based on field synergy principle and entropy generation analysis *Int J Heat Mass Transf* **68** 224–33

[6]   Li YF, Xia GD, Ma DD, Jia YT, and Wang J 2016 Characteristics of laminar flow and heat transfer in microchannel heat sink with triangular cavities and rectangular ribs *Int J Heat Mass Transf* **98** 17–28.

[7]   Japar WMAA, Sidik NAC and Mat S 2018 A comprehensive study on heat transfer enhancement in microchannel heat sink with secondary channel *Int Commun Heat Mass Transf* **99** 62–81.

[8]   A. Sahak AS, Che Sidik NA, and Akmal Yusof SN 2020 A Brief Review of Particle Dispersion of Cavity Flow *J. Adv. Res. App. Sc. Eng. Tech* **20(1)** 27-41

[9]   Aziz Japar WMA, Che Sidik NA, Aid SR, Asako Y, and Lit Ken T 2018 A Comprehensive Review on Numerical and Experimental Study of Nanofluid Performance in Microchannel Heatsink (MCHS) *J. Adv. Res. Fluid Mech. Therm. Sc.* **45(1)** 165-76.

[10] Aziz Japar WMA, Che Sidik NA, Saidur R, Asako Y, and Mohd Azmi MI 2019 Temperature Minimization on the Substrate of a Heat Sink By Rib-Groove Microchannel Heat Sink with Effective Energy Consumption: Groove Geometry Parameter Effects. *CFD Lett.* **11(9)** 1-13.

[11] Steinke ME, and Kandlikar SG 2006 Single-phase liquid friction factors in microchannels *Int J Therm Sci* **45(11)** 1073–83.

Acknowledgements